THE JOURNAL OF BIOLOGICAL CHEMISTRY
Vol. 280, No. 18, Issue of May 6, pp. 17945–17952, 2005
Printed in U.S.A.


# Functional Characterization of the MENTAL Domain*

Received for publication, January 20, 2005, and in revised form, February 17, 2005
Published, JBC Papers in Press, February 17, 2005, DOI 10.1074/jbc.M500723200

**Fabien Alpy‡§, Vinoth K. Latchumanan‡, Valérie Kedinger‡¶, Agnes Janoshazi‡, Christoph Thiele‖, Corinne Wendling‡, Marie-Christine Rio‡, and Catherine Tomasetto‡****

*From the ‡Institut de Génétique et de Biologie Moléculaire et Cellulaire (IGBMC), Département de Pathologie Moléculaire, UPR 6520 CNRS/U596 INSERM/Université Louis Pasteur, BP10142, 67404 Illkirch, C. U. de Strasbourg, France and ‖Max-Plank-Institute of Molecular Cell Biology and Genetics, Pfotenhauerstrasse 108, 01307 Dresden, Germany*

**Human metastatic lymph node (MLN) 64 is composed of two conserved regions. The amino terminus contains a conserved membrane-spanning MENTAL (MLN64 $NH_2$-terminal) domain shared with an unique protein called MENTHO (MLN64 $NH_2$-terminal domain homologue) and targets the protein to late endosome. The carboxyl-terminal domain is composed of a cholesterol binding steroidogenic acute regulatory-related lipid transfer domain exposed to the cytoplasm. MENTHO overexpression leads to the accumulation of enlarged endosomes. In this study, we show that MLN64 overexpression also induces the formation of enlarged endosomes, an effect that is probably mediated by the MENTAL domain. Using an *in vivo* photocholesterol binding assay, we find that the MENTAL domain of MLN64 is a cholesterol binding domain. Moreover, glutathione *S*-transferase pull-down or co-immunoprecipitation experiments demonstrate that this domain mediates homo- and hetero-interaction of MLN64 and MENTHO. In living cells, the expression of paired yellow fluorescent and cyan fluorescent fusion proteins show MENTHO homo-interaction and its interaction with MLN64. These data indicate that within late-endosomal membranes, MLN64 and MENTHO define discrete cholesterol-containing subdomains. The MENTAL domain might serve to maintain cholesterol at the membrane of late endosomes prior to its shuttle to cytoplasmic acceptor(s).**

Human metastatic lymph node (MLN)[1] 64 presents a correlated pattern of gene amplification and transcript overexpression in breast cancers and cancer-derived cell lines (1–6). MLN64 cDNA encodes a protein of 445 residues that can be divided into two halves. The amino-terminal half of the protein contains four potential transmembrane regions and targets the protein to the membrane of late endosomes, and the carboxyl-terminal half includes a sterol binding domain (7, 8).

Cells use endocytosis to internalize plasma membrane, surface receptors, and their ligands, viruses, and various extracellular molecules (9, 10). The endocytic pathway is critical for the correct sorting of proteins and lipids to their destination. The endocytic organelles could be divided into early (sorting and recycling endosomes) and late endosomes (late endosomes and lysosomes). Sorting decisions are made at every stage of the endocytic pathway and involve for transmembrane proteins the presence of specific targeting motifs such as dileucine- or tyrosine-based signals (11). The sorting of lipids is less understood. In normal cells, the intracellular cholesterol homeostasis is tightly regulated by an equilibrium between endogenous and exogenous sources (12). Exogenous cholesterol is mainly provided to the cells by circulating low density lipoproteins (LDL). LDL particle contains cholesterol esters in their core and are routed to late endosomes and lysosomes where the LDL particle is degraded and the cholesterol ester is deesterified by acid hydrolases. Free cholesterol egresses from this compartment principally to the plasma membrane (13).

The carboxyl-terminal half of MLN64 is structurally related to the steroidogenic acute regulatory (StAR) protein (7). StAR is a mitochondrial protein that regulates the acute production of steroids in the adrenal glands and gonads in response to corticotropin and luteinizing hormone, respectively (14). The functional relationship between MLN64 and StAR was previously addressed. It was shown that, similar to StAR, MLN64 can enhance steroidogenesis *in vitro* (15). Moreover, the region conserved between StAR and MLN64, the StAR-related lipid transfer (START) domain, was shown to be a cholesterol binding domain for both proteins (8). Although StAR acts as a sterol-carrier directly on the mitochondria (16, 17), MLN64 is likely to be involved in cholesterol transport from endosome to cytoplasmic acceptor(s) (18).

While searching for MLN64-related proteins, we isolated a novel late-endosomal protein, MENTHO (MLN64 $NH_2$-terminal domain homologue), which is structurally related to the amino-terminal half of MLN64. MENTHO and MLN64 share 70% identity and 83% similarity in a novel protein domain that we designated MENTAL (MLN64 $NH_2$-terminal) (19). Both genes share a ubiquitous expression pattern (7, 19). We previously showed that this domain was probably involved in the endocytic compartment dynamic since overexpression of MENTHO led to the accumulation of giant endosomes (19). Moreover, others have found that the deletion of the START domain

* This work was supported by funds from the Institut National de la Santé et de la Recherche Médicale (INSERM), Centre National de la Recherche Scientifique (CNRS), Université Louis Pasteur (ULP), and the Lique Nationale Contre le Cancer Comités du Haut-Rhin et du Bas-Rhin and from the Association pour la Recherche sur le Cancer (ARC). The costs of publication of this article were defrayed in part by the payment of page charges. This article must therefore be hereby marked "*advertisement*" in accordance with 18 U.S.C. Section 1734 solely to indicate this fact.

§ Recipient of an Association pour la Recherche sur le Cancer (ARC) fellowship.

¶ Recipient of a Fondation pour la Recherche Medicale (FRM) fellowship.

** To whom correspondence should be addressed: IGBMC, 1 rue Laurent Fries, BP 10142, 67404 Illkirch Cedex, France. Tel.: 33-3-88-65-35-19; Fax: 33-3-88-65-32-01; E-mail: cat@igbmc.u-strasbg.fr.

[1] The abbreviations used are: MLN, metastatic lymph node; MENTAL, MLN64 $NH_2$-terminal; MENTHO, MLN64 $NH_2$-terminal domain homologue; GST, glutathione *S*-transferase; CFP, cyan fluorescent protein; ECFP, enhanced CFP; YFP, yellow fluorescent protein; EYFP, enhanced YFP; FRET, fluorescence resonance energy transfer; $FRET^c$, corrected FRET; LDL, low density lipoprotein; TEV, tobacco etch virus; PBS, phosphate-buffered saline; StAR, steroidogenic acute regulatory; START, StAR-related lipid transfer; NLS, nuclear localization signal; GFP, green fluorescent protein; NPC, Niemann Pick C; rTEV, recombinant TEV.

within the MLN64 protein was responsible for a similar phenotype (20).

The roles of MLN64 and MENTHO remain elusive. Because the MENTAL domain is present only in these two proteins, we postulated that this region is important for their function. Therefore, we undertook the molecular and functional characterization of the MENTAL domain.

## EXPERIMENTAL PROCEDURES

*Cloning and Constructs*—Plasmids pSG5-MLN64, pSG5-MENTHO, pRK7N-MENTHO, pEGFPC2-MENTHO, pCR3.1-NPC1, and pEGFP-NET-NLS allowing the expression of MLN64 (MLN64-(1–445)) and MENTHO, FLAG-MENTHO, and GFP-MENTHO, respectively, were previously described (18, 19). pSG5-MLN64-(1–218), pSG5 MLN64-(1–171), pSG5-MLN64-(47–445), and pat4-MLN64Δ1–234 allowing the expression of MLN64-(1–218), MLN64-(1–171), MLN64-(47–445), MLN64-(235–445), Niemann Pick C1 (NPC1), and nuclear-GFP, respectively, were described previously (7, 18, 19).

A construct allowing the expression of GST-tagged MLN64 protein (GST-MLN64) was generated as follows. A 733-bp fragment was amplified by PCR using the synthetic oligonucleotides, 5′-GAG AGT CGA CTA TGA ACC ACC TGC CAG AAG ACA TGG-3′ and 5′-TCT CGT CGA CGT AGT ACT CAT AGT TCT AAA AGT GG-3′, incorporating in-frame NheI restriction sites. This cDNA fragment was released by NheI digestion and inserted in-frame behind the GST coding sequence in the pBC vector (BD Biosciences), thus generating pBC-MLN64. To incorporate a specific cleavage site for the tobacco etch virus (TEV) protease (ENLYFNG) between the MENTAL and START domains of MLN64, the pBC-MLN64 was mutated by site-directed mutagenesis site at position 181–187 using the synthetic oligonucleotide, 5′-GGA AGC TGA AGA GGA GAA CCT GTA TTT TCA GGG CCA GGT TGC TG-3′ (QuikChange site-directed mutagenesis kit, Stratagene), thus generating pBC-MLN64-rTEV.

Plasmids coding for fluorescent fusion proteins used for fluorescence resonance energy transfer (FRET) experiments were generated as follows. A cDNA fragment corresponding to the MENTHO open reading frame was obtained by PCR amplification using the synthetic oligonucleotides containing XbaI restriction sites, 5′-GAG ATC TAG AAT GAA CCA CCT GCC AGA AGA C-3′ and 5′-GAG ATC TAG ACC TAG TTC TAA AAG TGG TTT CTC ACT-3′, and cloned in-frame into the NheI site of the pEYFP-C1 vector (BD Biosciences, Clontech) upstream of the YFP, thus generating the vector pEYFP-NheI-MENTHO allowing the expression of the MENTHO-YFP fusion protein. Similarly, after PCR amplification using the synthetic oligonucleotides, 5′-GAG ACA ATT GTA ACC ACC TGC CAG AAG ACA TG-3′ and 5′-GAG ACA ATT GTC ATA GTT CTA AAA GTG GTT TCT CAC-3′, the modified MENTHO cDNA was digested by MunI and cloned in-frame into the EcoRI site of the pEYFP-C1 vector behind the EYFP cDNA sequence, thus generating the vector pEYFP-EcoRI-MENTHO allowing the expression of the YFP-MENTHO fusion protein. Similarly, the vector pECFP-NheI-MENTHO allowing the expression of the MENTHO-cyan fluorescent protein (CFP) fusion protein was obtained by PCR amplification using the synthetic oligonucleotides, 5′-GAG ATC TAG AAT GAA CCA CCT GCC AGA AGA C-3′ and 5′-GAG ATC TAG ACC TAG TTC TAA AAG TGG TTT CTC ACT-3′, incorporating flanking XbaI sites and cloned in-frame into the NheI site of the pECFP-C1 vector. A plasmid encoding a double fusion protein CFP-MENTHO-YFP was also generated by PCR amplification using the synthetic oligonucleotides, 5′-GAG ACA ATT GCG AGA ACG CTC TCA CCG GGA GC-3′ and 5′-GAG ACA ATT GTC ACT TGT ACA GCT CGT CCA TGC C-3′, and pEYFP-NheI-MENTHO as template. The modified cDNA encoding the MENTHO-YFP protein was digested by MunI and cloned in-frame into the EcoRI site of the pECFP-C1 vector behind the ECFP cDNA sequence, thus generating the vector pECFP-MENTHO-YFP allowing the expression of the CFP-MENTHO-YFP double fusion protein. The plasmid pSG5-MLN64 was mutated to contain a EcoRI site by site-directed mutagenesis using the synthetic oligonucleotide, 5′-CGA GCT GGG GGC CCG GGG AAT TCT GTG CCC CCT CCC AC-3′. A DNA fragment containing MLN64 open reading frame was then excised by EcoRI digestion and cloned in-frame into the EcoRI site of the pEYFP-N1 vector (BD Biosciences, Clontech), thus generating the vector pEYFP-MLN64 allowing the expression of the MLN64-YFP fusion protein.

The complete open reading frames of STARD4 (GenBank™ accession number AF_480299) was cloned by RT-PCR using HeLa cell single strand cDNA as template and the following primers, 5′-GAA GTA ATG GAA GGC CTG TCT GAT GTT G-3′ and 5′-TCA TAA AGC TTT TCG TAA ATC ACC-3′. PCR products were cloned into the pCR3.1 expression vector (BD Biosciences), generating the pCR3.1 STARD4 plasmid. After PCR amplification using primers containing flanking MunI sites, the STARD4 coding sequence was digested by MunI and cloned in-frame into the EcoRI site of the pEYFP-C1 vector, thus generating the vector pEYFP-STARD4 allowing the expression of the YFP-STARD4 fusion protein. Constructs coding for GFP-Rab5a and GFP-Rab7 fusion proteins were obtained similarly. The complete open reading frames of Rab5a (GenBank™ accession number NM_004162) and Rab7 (GenBank™ accession number NM_004637) were obtained by RT-PCR using NPC2 cell single strand cDNA as template and the following primers containing flanking MunI sites, 5′-GAG ACA ATT GGC TAG TCG AGG CGC AAC AAG ACC CAA CG-3′, 5′-GAG ACA ATT GTT AGT TAC TAC AAC ACT GAT TCC TGG TTG G-3′ and 5′-GAG ACA ATT GAC CTC TAG GAA GAA AGT GTT GCT GAA GG-3′, and 5′-GAG ACA ATT GTC AGC AAC TGC AGC TTT CTG CCG AGG CC-3′, respectively. PCR products were digested by MunI and cloned into the pEGFP-C2 expression vector (BD Biosciences, Clontech), generating the pEGFP-Rab5a and pEGFP-Rab7 vectors, respectively.

*Antibodies*—The rabbit polyclonal 605 (pAbMLN64-Ct), the mouse monoclonal 2BE2F4 (mAbMLN64-Ct), and the rabbit polyclonal antibody 1611 (pAbMLN64-Nt) directed against MLN64 have been described (18). The rabbit polyclonal 1546 antibody (pAbMENTHO-Ct) directed against MENTHO has been described (19). The monoclonal anti-FLAG M2 or polyclonal anti-FLAG antibodies were from Sigma. The rabbit polyclonal anti-GFP was from Clinisciences (Montrouge, France). The rabbit polyclonal anti-NPC1 and anti-NPC2 antibodies were described previously (21, 22).

*Immunocytofluorescence*—HeLa cells were grown to 70% confluence on glass coverslips. After washing with phosphate-buffered saline (PBS), cells were fixed for 10 min at room temperature in 4% paraformaldehyde in PBS and permeabilized for 10 min with 0.1% Triton X-100 in PBS. After blocking in 1% bovine serum albumin in PBS, cells were incubated at room temperature with the primary antibodies for 1 h. Cells were washed three times in PBS and incubated for 1 h with CY3-conjugated affinity-purified donkey anti-rabbit IgG (Jackson ImmunoResearch Laboratories, Inc., West Grove, PA). Cells were washed three times in PBS, and nuclei were counterstained with Hoechst-33258 dye. Slides were mounted in Aqua Poly/Mount (Polysciences, Inc., Warrington, PA). Observations were made with a confocal microscope (Leica TCS SP1, Heidelberg, Germany).

*Immunoprecipation, GST Pull-down, and Immunoblotting*—For co-immunoprecipitation and GST pull-down, HeLa cells ($2 \times 10^6$) were plated on 10-cm dishes and transfected using JetPEI™ transfection reagent (Polyplus transfection, Illkirch, France) with a total of 10 $\mu$g of DNA containing various expression plasmids. After 24 h, cells were washed twice in serum-free medium and incubated for 24 h in complete medium. Cells were collected and washed once in PBS. Lysis was performed by incubating the cells for 15 min at 4 °C in 300 $\mu$l of lysis buffer (50 mM Tris-HCl, pH 7.5, 150 mM NaCl, 1 mM EDTA, 1% Triton X-100, and protease inhibitor mixture). Cellular debris were removed by centrifugation at 10,000 $\times$ *g* for 10 min.

1 mg of total protein extract was incubated for 10–12 h at 4 °C with 40 $\mu$l of anti-FLAG M2 monoclonal antibody affinity resin (Sigma) or with 40 $\mu$l of glutathione-agarose beads (glutathione-agarose 4B, Amersham Biosciences) for co-immunoprecipitation and GST pull-down, respectively. The beads were washed extensively with lysis buffer or, when indicated, with lysis buffer containing 1 M NaCl or with radioimmune precipitation buffer (1× PBS, 0.1% SDS, 0.5% Nonidet P-40, and 0.5% sodium deoxycholate). Bound proteins were eluted by SDS sample buffer (50 mM Tris-HCl, pH 6.8, SDS 2%, glycerol 10%, β-mercaptoethanol, and 1.4 M, bromphenol blue). Eluted proteins were recovered from the beads by centrifugation. Total proteins and eluted proteins were resolved by 8–15% SDS-PAGE and electrotransferred to nitrocellulose sheets (Schleicher & Schuell, Dassel, Germany). The membrane was blocked in PBS containing 3% nonfat dry milk and 0.1% Tween 20 and then incubated with the primary antibody. After washing, the blots were incubated with appropriate secondary antibodies. Horseradish peroxidase-conjugated AffiniPure donkey anti-rabbit or goat anti-mouse at 1/10,000 (Jackson ImmunoResearch) was used. Finally, protein-antibody complexes were visualized by an enhanced chemiluminescence detection system (SuperSignal West Pico, Pierce).

*Interaction of the MENTAL Domain and Photocholesterol*—HeLa cells ($2 \times 10^6$) were plated on 10-cm dishes and transfected using JetPEI transfection reagent as described above. 48 h after transfection, cells were labeled with [$^3$H]photocholesterol. [$^3$H]Photocholesterol differs from cholesterol, because it lacks the Δ5 double bond and the hydrogen at C-6, which are replaced by the photoactivatable diazirine ring, and is tritiated at the 3α position (23). [$^3$H]Photocholesterol dis-

solved in ethanol was loaded into fetal calf serum by injecting a concentrated [$^3$H]photocholesterol solution into stirred serum at 37 °C followed by stirring for 1 h. Final ethanol concentration was <0.2%. Precipitates were removed by a 100,000 × *g* centrifugation for 1 h, and the serum was filtered through a 0.2-$\mu$m filter. Human plasma that was treated the same way showed nearly exclusive labeling of LDL and high density lipoprotein (23). The resulting serum containing [$^3$H]photocholesterol had an activity of 700 $\mu$Ci/ml. 4 ml of medium (Dulbecco's modified Eagle's medium) supplemented with 150 $\mu$l of serum containing [$^3$H]photocholesterol were added to each dish. 16 h later, cells were washed twice with PBS, fed with PBS supplemented with delipidated fetal calf serum, and then irradiated for 20 min at 4 °C under UV light using the filtered (340 ± 40 nm) beam of a high-pressure 100-watt mercury lamp. Protein extracts were then prepared as described above. When needed, rTEV digestion was performed according to the manufacturer's instructions (Invitrogen). Fluorography was performed with the Amplify fluorographic reagent (Amersham Biosciences) according to the manufacturer's instructions.

*FRET*—HeLa cells were plated onto 35-mm glass bottom dishes (MatTek, Ashland, MA). Cells were transfected with JetPei reagent 2 days before the experiment. After replacement of the cell culture medium by PBS, confocal fluorescence microscopy was done on a SP2 AOBS microscope (Leica, Wetzlar, Germany). For the image series and spectra measurements, a Leica TSC SP2-AOBS equipped with an acousto-optical beamsplitter and argon and helium-neon lasers were used with a ×63/1.4 oil immersion objective. To visualize the spatial distribution of the proteins and their FRET, three images (donor, FRET, and acceptor) were acquired in the same order in all of the experiments. As excitation source, CFP was excited at 458 nm, YFP was excited at 514 nm, and emissions were detected between 465 and 500 and 525 and 600 nm for CFP (donor) and YFP (acceptor) channels, respectively. Raw FRET images were obtained by using a 458-nm laser line for donor excitation and detecting the FRET emission in the interval of 525–600 nm with the same set up parameters as we used for detecting the emission of CFP and YFP.

Calculations of corrected FRET (FRET$^c$) in the FRET channel were carried out on a pixel-by-pixel basis for the entire image. The bleedthrough of CFP and YFP through the FRET emission channel was regarded by using the following equation: FRET$^c$ = FRET − (bleedthrough CFP × CFP) − (direct excitation by 458 nm of YFP × YFP) − autofluorescence. The FRET$^c$ intensity values were then normalized to the amounts of CFP donor and YFP acceptor present by the product CFP × YFP. FRET$^c$ values as FRET efficiency are represented as the mean ± S.E. To evaluate the bleedthrough of CFP and the direct excitation of YFP by 458 nm, we used calibration curves calculated from the measurements of the single labeled cells. The overall intensity of FRET was calculated using SigmaPlot and house-made softwares. FRET$^c$ images are displayed as YFP intensity-modulated images in pseudo-color mode where the red areas display high values of FRET and blue areas display low values of FRET.

The quantitative method that we have used was the sensitized emission method. This approach requires excitation of the donor and then detection of the emission spectrum of the donor-acceptor. Spectral deconvolution, which gives the corrections for spectral overlap between CFP and YFP, was performed first after background subtraction and then FRET efficiency was calculated according to Xia *et al.* (24). Images in CFP (excitation 458 nm) and YFP (excitation 514 nm) channels have to be recorded prior the spectral measurements for the FRET efficiency calculations. Single labeled cells were used to estimate the optimal conditions to avoid direct excitation of YFP by the 458-nm excitation and record the spectral shape of the donor and acceptor for deconvolution of the FRET spectra. Thus, spectral imaging can take full advantage of fluorescent indicator dyes that undergo spectral changes and will provide an accurate quantitative indicator for FRET efficiency calculation. Statistical analysis was performed by using Student's *t* test assuming that standard deviation index values showed normal distributions (SigmaPlot software).

## RESULTS

*MLN64 and MENTHO Interaction*—The MENTAL domain contains four transmembrane helices spanning the membrane of late endosomes (19). Its structural organization resembles that of tetraspanin proteins, a large family of integral membrane proteins involved in cell motility, fusion, and signaling. As tetraspanins associate extensively with one another and with other transmembrane and membrane-proximal proteins, we hypothesized that MLN64 and MENTHO might dimerize to

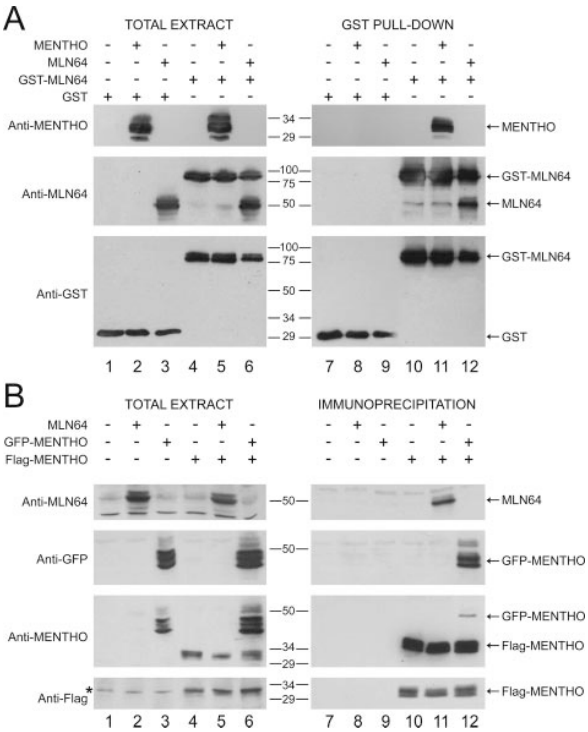


FIG. 1. **MLN64 and MENTHO homo- and hetero-dimerize.** *A*, HeLa cells were transfected with plasmids encoding GST (*lanes 1–3* and *7–9*), MENTHO (*lanes 2*, *5*, *8*, and *11*), MLN64 (*lanes 3*, *6*, *9*, and *12*), and GST-MLN64 (*lanes 4–6* and *10–12*). Protein extracts were subjected to GST pull-down using glutathione-agarose beads. Total protein extracts (*left panel*) and bound proteins (*right panel*) were analyzed by Western blot using anti-MENTHO, anti-MLN64, and anti-GST antibodies. *B*, HeLa cells were transfected with a control empty vector (*lanes 1* and *7*) or with plasmids encoding MLN64 (*lanes 2*, *5*, *8*, and *11*), GFP-MENTHO (*lanes 3*, *6*, *9*, and *12*), and FLAG-MENTHO (*lanes 4–6* and *10–12*). Protein extracts were subjected to immunoprecipitation using mouse anti-FLAGM2 affinity resin. Total protein extracts (*left panel*) and bound proteins (*right panel*) were analyzed by immunoblot using anti-MLN64, anti-GFP, anti-MENTHO, and anti-FLAG antibodies. The protein molecular size markers are indicated in between the blots. The relative size of the proteins is indicated on the *right*.

form complexes at the membrane of endosomes. To address this question, we performed GST pull-down and immunoprecipitation assays (Fig. 1). Plasmids encoding the GST-MLN64 fusion protein and MENTHO or MLN64 were co-transfected into human HeLa cells. MENTHO and MLN64 were specifically immunoprecipitated with GST-MLN64 but not with GST alone. This experiment showed that MLN64 can form homo-oligomers and hetero-oligomers with MENTHO (Fig. 1*A*). To confirm these interactions, the complementary experiment was performed. Plasmids encoding FLAG-tagged MENTHO and MLN64 or GFP-MENTHO were transiently expressed in HeLa cells. Immunoprecipitated FLAG-tagged complexes analyzed by immunoblotting showed that MLN64 and GFP-MENTHO were specifically immunoprecipitated with FLAG-MENTHO (Fig. 1*B*).

Because MLN64 and MENTHO are membrane proteins, we verified that the observed interactions were not caused during the preparation of the protein lysates by detergent-induced co-precipitation. Plasmids coding for FLAG-MENTHO or MLN64 were individually transfected in HeLa cells. Cellular lysates were mixed and subjected to anti-FLAG immunoprecipitation as described above. Under this experimental condition, the immunoprecipitates showed no interaction between FLAG-MENTHO and MLN64 (Fig. 2*A*). To evaluate the stability of the interaction between MLN64 and MENTHO, HeLa

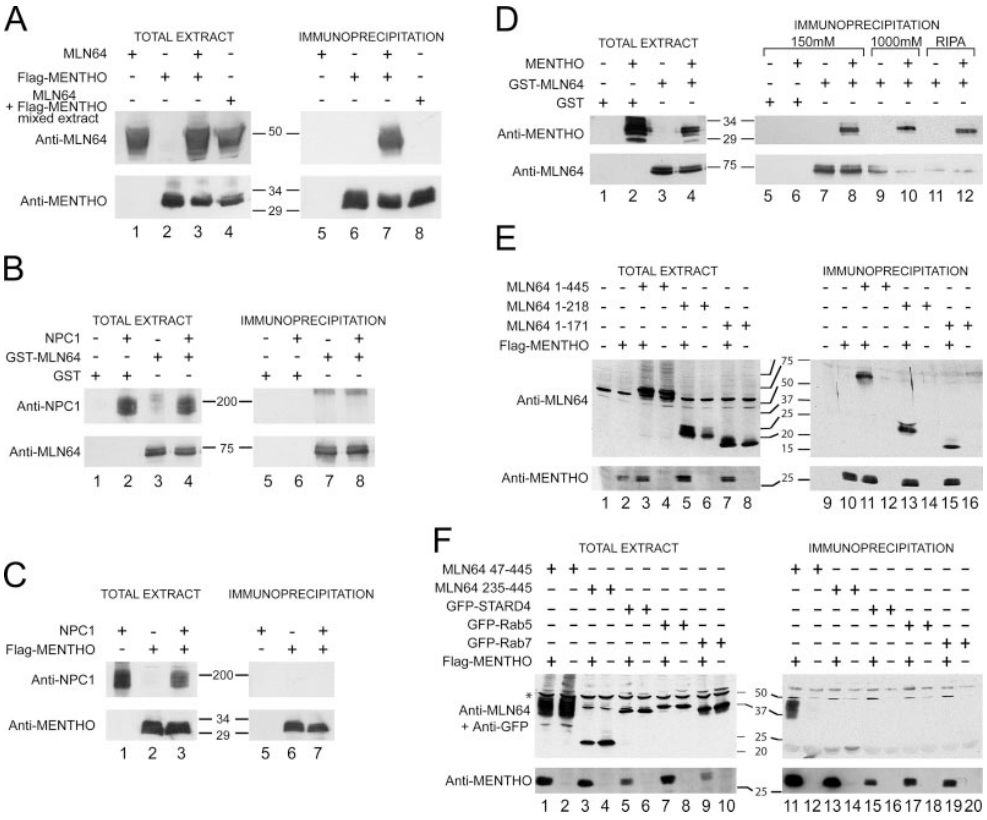


FIG. 2. **The MENTAL domain of MLN64 and MENTHO mediates their interaction.** *A*, HeLa cells were transfected with MLN64 (*lanes 1* and *5*) and FLAG-MENTHO (*lanes 2* and *6*) or co-transfected with FLAG-MENTHO and MLN64 (*lanes 3* and *7*) encoding vectors. Separate cellular lysates containing either MLN64 or FLAG-MENTHO were mixed together (*lanes 4* and *8*). Protein extracts were subjected to immunoprecipitation using mouse anti-FLAG antibody. Total protein extracts (*left panel*) and bound proteins (*right panel*) were analyzed by Western blot using anti-MLN64, anti-GFP, anti-MENTHO, and anti-FLAG antibodies. *B*, HeLa cells were transfected with GST (*lanes 1* and *5*), GST and NPC1 (*lanes 2* and *6*), GST-MLN64 (*lanes 3* and *7*), and GST-MLN64 and NPC1 (*lanes 4* and *8*) encoding vectors. Protein extracts were subjected to GST pull-down. Total protein extracts (*left panel*) and bound proteins (*right panel*) were analyzed by Western blot using anti-NPC1 and anti-MLN64 antibodies. *C*, HeLa cells were transfected with NPC1 (*lanes 1* and *5*), FLAG-MENTHO (*lanes 2* and *6*), and NPC1 plus FLAG-MENTHO (*lanes 3* and *7*) encoding vectors. Protein extracts were subjected to immunoprecipitation using anti-FLAG antibodies. Total protein extracts (*left panel*) and immunoprecipitated proteins (*right panel*) were analyzed by Western blot using anti-NPC1 and anti-MENTHO antibodies. *D*, HeLa cells were transfected with GST (*lanes 1* and *5*), GST and MENTHO (*lanes 2* and *6*), GST-MLN64 (*lanes 3*, *7*, *9*, and *11*), and GST-MLN64 and MENTHO (*lanes 4*, *8*, *10*, and *12*) encoding vectors. Protein extracts were subjected to GST pull-down. Washes were performed with different NaCl concentrations (150 mM and 1 M) or with radioimmune precipitation (*RIPA*) buffer (137 mM sodium chloride, 10 mM phosphate, 2.7 mM potassium chloride, 0.1% SDS, 0.5% Nonidet P-40, and 0.5% sodium deoxycholate, pH 7.4). Total protein extracts (*left panel*) and bound proteins (*right panel*) were analyzed by Western blot using anti-MENTHO and anti-MLN64 antibodies. *E*, HeLa cells were transfected with empty vector (*lanes 1* and *9*), FLAG-MENTHO (*lanes 2*, *3*, *5*, *7*, *10*, *11*, *13*, and *15*), MLN64 1–445 (*lanes 3*, *4*, *11*, and *12*), MLN64 1–217 (*lanes 5*, *6*, *13*, and *14*), and MLN64 1–171 (*lanes 7*, *8*, *15*, and *16*) encoding vectors. Protein extracts were subjected to immunoprecipitation using a mouse anti-FLAG antibody. Total protein extracts (*left panel*) and bound proteins (*right panel*) were analyzed by Western blot using anti-MLN64 and anti-MENTHO antibodies. *F*, HeLa cells were transfected with FLAG-MENTHO (*lanes 1*, *3*, *5*, *7*, *9*, *11*, *13*, *15*, *17*, and *19*), MLN64 45–445 (*lanes 1*, *2*, *11*, and *12*), MLN64 235–445 (*lanes 3*, *4*, *13*, and *14*), GFP-STARD4 (*lanes 5*, *6*, *15*, and *16*), GFP-Rab5 (*lanes 1*, *7*, *8*, and *18*), and GFP-Rab7 (*lanes 9*, *10*, *19*, and *20*) encoding vectors. Protein extracts were subjected to immunoprecipitation using mouse anti-FLAG antibody. Total protein extracts (*left panel*) and bound proteins (*right panel*) were analyzed by Western blot using anti-MLN64 and anti-GFP antibodies (*upper panel*) or anti-MENTHO antibodies (*lower panel*). The *asterisk* indicates a nonspecific signal. The protein molecular size markers are indicated between the blots (in kDa).

cells were co-transfected with GST-MLN64- and MENTHO-encoding vectors and GST-pull down complexes were subjected to stringent washes with 1 M NaCl-containing buffer (Fig. 2*D*, *lanes 9* and *10*) or with a 0.1% SDS-containing buffer (Fig. 2*D*, *lanes 11* and *12*). The interaction between MLN64 and MENTHO was resistant to these stringent conditions (Fig. 2*D*).

To study the specificity of the interaction between MLN64 and MENTHO, we looked at their interaction with another membrane-spanning protein from late endosomes, the NPC1 protein. GST-MLN64 and NPC1 or FLAG-MENTHO and NPC1 were transiently expressed in HeLa cells. NPC1 was not pulled down with GST-MLN64 (Fig. 2*B*) or co-immunoprecipitated with FLAG-MENTHO (Fig. 2*C*). Similarly, MENTHO did not interact with NPC2 (data not shown), a GFP-STARD4 fusion protein, GFP-Rab5, or GFP-Rab7 fusion proteins (Fig. 2*F*). When expressed in HeLa cells, the GFP-STARD4 fusion protein gave a diffuse cytosolic and nuclear signal (data not shown). Thus, we detected no direct interaction between MENTHO and cytosolic vesicular-associated proteins like Rab5 or Rab7, the cytosolic protein STARD4, or the intraluminal lysosomal protein, NPC2. Altogether, these results show that MLN64 and MENTHO interact specifically with each other.

*The MENTAL Domain of MLN64 and MENTHO Mediates Their Interaction*—To map the region of MLN64 mediating the interaction between MLN64 and MENTHO, plasmids coding for truncated MLN64 proteins were co-transfected with a plasmid encoding FLAG-MENTHO. Immunoprecipitated complexes with anti-FLAG antibody resin were analyzed by Western blot analysis. MLN64-(1–218) and MLN64-(1–172) proteins deleted at the COOH-terminal part were immunoprecipitated similarly to the wild-type protein (Fig. 2*E*). A mutant protein containing a short amino-terminal deletion, MLN64-(47–445),

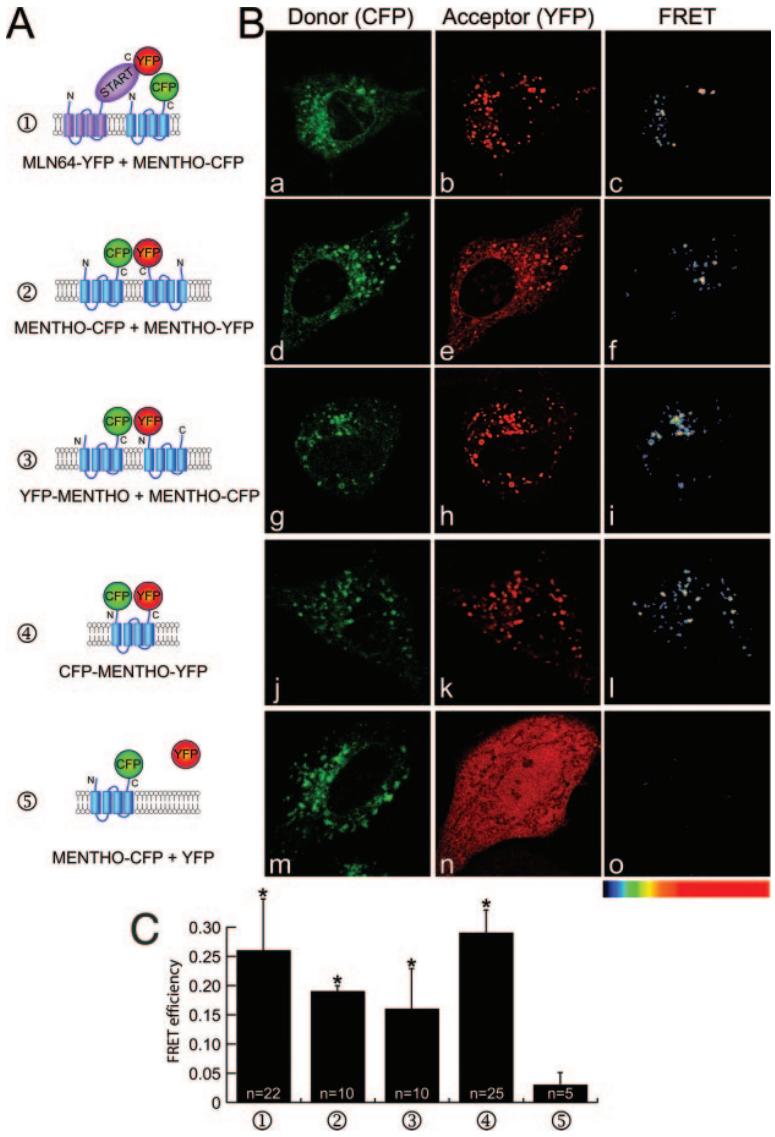


FIG. 3. **MLN64 and MENTHO interact in living cells.** *A*, scheme of the different combinations of MLN64 and MENTHO proteins fused to CFP or YFP used as donor and acceptor for FRET experiments. *N* and *C* correspond to the amino and carboxyl termini of each protein, respectively. *B*, HeLa cells were transiently transfected with the expression vectors for the different fusion proteins described in *A*, MLN64-YFP and CFP-MENTHO (*B*, *a–c*), MENTHO-YFP and CFP-MENTHO (*B*, *d–f*), YFP-MENTHO and CFP-MENTHO (*B*, *g–i*), CFP-MENTHO-YFP (*B*, *j–l*), or CFP-MENTHO and YFP (*B*, *m–o*). The images corresponding to the CFP emission (*green*, *a*, *d*, *g*, and *j*), the YFP emission (*red*, *b*, *e*, *h*, and *k*), and the FRET were acquired with a confocal microscope on living cells. The corrected FRET images (*c*, *f*, *i*, and *l*) are displayed in pseudo-color mode where *blue* and *red areas* correspond to low and high values of FRET, respectively (*lower panel*). *C*, FRET efficiency for the different combination of YFP- and CFP-coupled proteins described in *A*. Corrected FRET values were obtained by subtracting the bleedthrough of CFP in the FRET channel and the direct excitation of YFP by the 458-nm light to the raw FRET measured. *n* corresponds to the number of cells from which the 100 co-localization points used for the quantification were taken. *, $p < 0.001$.

was also efficiently co-precipitated with MENTHO (Fig. 2*F*). On the contrary, a MLN64-mutant where the MENTAL domain was completely deleted and contained only the START domain, MLN64-(235–445), did not co-immunoprecipitate with MENTHO (Fig. 2*F*).

These results indicate that the MLN64 and MENTHO interaction is specific and that the region mediating this interaction lies within amino acids 47–171 of the MLN64 protein corresponding to the conserved MENTAL domain.

*MLN64 and MENTHO Interact in Living Cells*—To have *in vivo* evidence that MLN64 and MENTHO interact, we performed the FRET analysis. FRET exploits the capacity of the higher energy fluorophore (donor) to transfer energy when excited to a lower energy fluorophore (acceptor) when these two molecules are closer than 10 nm. Thus, the binding of two fluorescence-tagged proteins can be detected by measuring the emission intensity of the acceptor fluorophore after exciting the donor fluorophore. Proteins fused to cyan (CFP) and YFP, two variants of the enhanced green fluorescent protein, were used as donor and acceptor for the FRET pair, respectively. For quantitative FRET, we applied the sensitized emission method to excite the donor fluorochrome and the emission spectrum of the donor-acceptor pair was measured. FRET efficiency was calculated following background correction and bleedthrough calculation using a spectral deconvolution to allow CFP and YFP emission spectra separation (24).

HeLa cells were co-transfected with plasmids coding for CFP-MENTHO (CFP is fused to the amino-terminal end of MENTHO) and MLN64-YFP (YFP is fused to the carboxyl-terminal end of MLN64) fusion proteins. A strong FRET signal was observed in endosomes, indicating close proximity of these two proteins (Fig. 3, *A1* and *B*, *a–c*). The FRET efficiency was $0.26 \pm 0.09$ close to the maximal FRET efficiency of the CFP-YFP pair (Fig. 3*C*). We then confirmed that MENTHO can self-interact. HeLa cells were co-transfected with plasmids coding for CFP-MENTHO and MENTHO-YFP (Fig. 3, *A2* and *B*, *d–f*) or YFP-MENTHO (Fig. 3, *A3* and *B*, *g–i*). In both cases, FRET occurred with an efficiency of $0.19 \pm 0.01$ and $0.16 \pm 0.07$, respectively. When cells expressed CFP-MENTHO and YFP alone (Fig. 3, *A5* and *B*, *m–o*), no significant FRET was obtained (Fig. 3*C*). Finally, as a positive control, we analyzed cells expressing the CFP-MENTHO-YFP where MENTHO is fused to CFP and YFP at its amino and carboxyl termini, respectively (Fig. 3*A4* and *B*, *j–l*). The very high FRET efficiency of the CFP-MENTHO-YFP fusion protein ($0.29 \pm 0.04$) indicates a close intramolecular or intermolecular proximity of

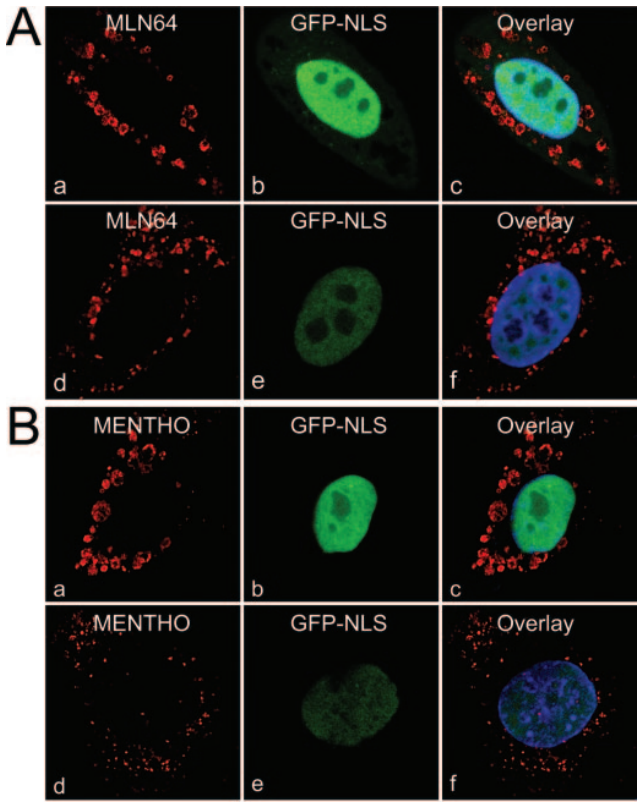


FIG. 4. **The overexpression of the MENTAL domain of MLN64 and MENTHO induces the formation of giant endosomes.** Confocal sections were taken from HeLa cells transfected with pSG5-MLN64 and pGFP-NET-NLS (*A*) or with pSG5-MENTHO and pGFP-NET-NLS (*B*). Cells were stained with mAbMLN64 (*A*, *red*) or with pAbMENTHO (*B*, *red*). In *A* and *B*, nuclei were counterstained with Hoechst-33258 dye (*A*, *c* and *f*, and *B*, *c* and *f*, *blue*). The signals obtained using an identical setting of the microscope in cells synthesizing high and low levels of nuclear-GFP are shown in *b* (*green*) and *e* (*green*), respectively. Merged images of MLN64, GFP, and Hoechst-33258 dye signals are shown in *A*, *c* and *f*. Merged images of MENTHO, GFP, and Hoechst-33258 dye signals are shown in *B*, *c* and *f*.

the amino- and COOH-terminal ends of the MENTHO protein. All of these results suggest that MENTHO can dimerize to itself or is present in homo- and hetero-dimers (or oligomers) with MLN64 in living cells.

*Overexpression of the MENTAL Domain Induces Endosomal Enlargement*—We have previously showed that the overexpression of MENTHO in cells leads to an enlargement of endosomes (19). To evaluate whether MLN64 overexpression could also induce endosomal enlargement, HeLa cells were transfected with equal quantities of two expression vectors encoding the nuclear-GFP protein (GFP-NLS) and MLN64. GFP intensity was used to select for transfected cells and to assess the level of expression of the transfected vectors. Morphological changes in the endosomes were studied in cells showing either high or low GFP fluorescence (Fig. 4*A*). MLN64 labeling appeared in larger perinuclear endosomes in high GFP fluorescence cells (Fig. 4*A*, *a–c*), whereas it appeared in smaller scattered endosomes in low GFP fluorescence cells (Fig. 4*A*, *d–f*). A similar experiment using MENTHO and nuclear-GFP-co-expressing cells showed that MENTHO overexpression induced a perinuclear accumulation of less numerous but equally enlarged endosomes (Fig. 4*B*, *a–c*). In conclusion, high levels of MLN64 or MENTHO induced endosomal enlargement, suggesting that this feature is caused by their common MENTAL domain.

*The MENTAL Domain Binds Cholesterol*—MLN64 has been hypothesized to be involved in late endosome cholesterol transport. The carboxyl-terminal half-START domain binds cholesterol directly at an equimolar ratio (8). This domain projects toward the cytoplasm from the endosome membrane, whereas the amino-terminal MENTAL domain is anchored in the membrane (18). In order to reach the cytoplasmic START domain, cholesterol that is sequestered within endosomes must pass through the outer endosomal membrane. Therefore, we examined whether the MENTAL domain of MLN64 could retain cholesterol on its way to the cytoplasm.

The cholesterol binding properties of the MENTAL domain were studied *in vivo* using a photoactivable cholesterol analogue, [$^3$H]photocholesterol (23). HeLa cells were transfected either with a construct allowing the expression of a wild-type MLN64 fused with GST (GST-MLN64) or with a mutant GST-MLN64 construct in which a highly specific cleavage site (ENLYFNG) for the viral protease rTEV (25) was added by site-directed mutagenesis between the START and the MENTAL domains of MLN64 (GST-MLN64-rTEV) (Fig. 5*A*). Transfected HeLa cells synthesizing GST alone as negative control, GST-MLN64, or GST-MLN64-rTEV were then incubated with [$^3$H]photocholesterol (incorporated into LDL particles). Covalent binding with cholesterol was achieved by UV irradiation. Cells were then lysed and processed for GST pull-down assay. After purification, bound proteins were subjected to rTEV cleavage. The purified proteins and their cleaved products were analyzed by SDS-PAGE (Fig. 5*B*), and purified covalent cholesterol-protein complexes were visualized by fluorography (Fig. 5*C*). Both GST-MLN64 (*lanes 3*, *7*, and *11*) and GST-MLN64-rTEV (*lanes 4*, *8*, and *12*) were strongly labeled by the tritiated cholesterol analogue, whereas GST alone was not labeled (*lanes 2*, *6*, and *10*). To examine whether the MENTAL of MLN64 was involved in cholesterol binding, purified GST-MLN64-rTEV protein complexes were cleaved with the rTEV protease before SDS-PAGE and autoradiography (Fig. 5, *lane 12*). Under these conditions, the cleaved product containing only the MLN64 MENTAL domain was strongly labeled. All of these data show that MLN64 binds cholesterol *in vivo* via its transmembrane MENTAL domain.

## DISCUSSION

The aim of this study was to further the understanding of the function of human MLN64. Previous studies proposed that MLN64 was involved in cholesterol homeostasis and in steroidogenesis (7, 15, 18, 20, 26–28). Indeed, MLN64 could participate to cholesterol egress from late endosomes via the function of its cytoplasmic START domain.

In man, 15 distinct genes encoding proteins belonging to the START protein family have been found. In these proteins, START domains are either alone or in concert with other domains (29, 30). For instance, the CERT/STARD11 protein involved in the cytosolic transport of ceramide also contains a START domain in addition to a pleckstrin homology domain (31). CERT function depends on the presence of the START domain to handle ceramide, whereas the amino-terminal pleckstrin homology domain addresses the protein to the Golgi apparatus (31). MLN64 (STARD3) is a multidomain protein that contains both a MENTAL and a START domain. The functional relevance of this association was addressed.

The MENTAL domain is composed of four transmembrane helices with three short intervening loops (19). Another conserved transmembrane domain called the sterol-sensing domain is present in some of the proteins involved in cholesterol transport and homeostasis, such as NPC1 or sterol regulatory element-binding protein cleavage-activating protein. The sterol-sensing domain consists of ~180 amino acids that form five predicted membrane-spanning helices with short intervening

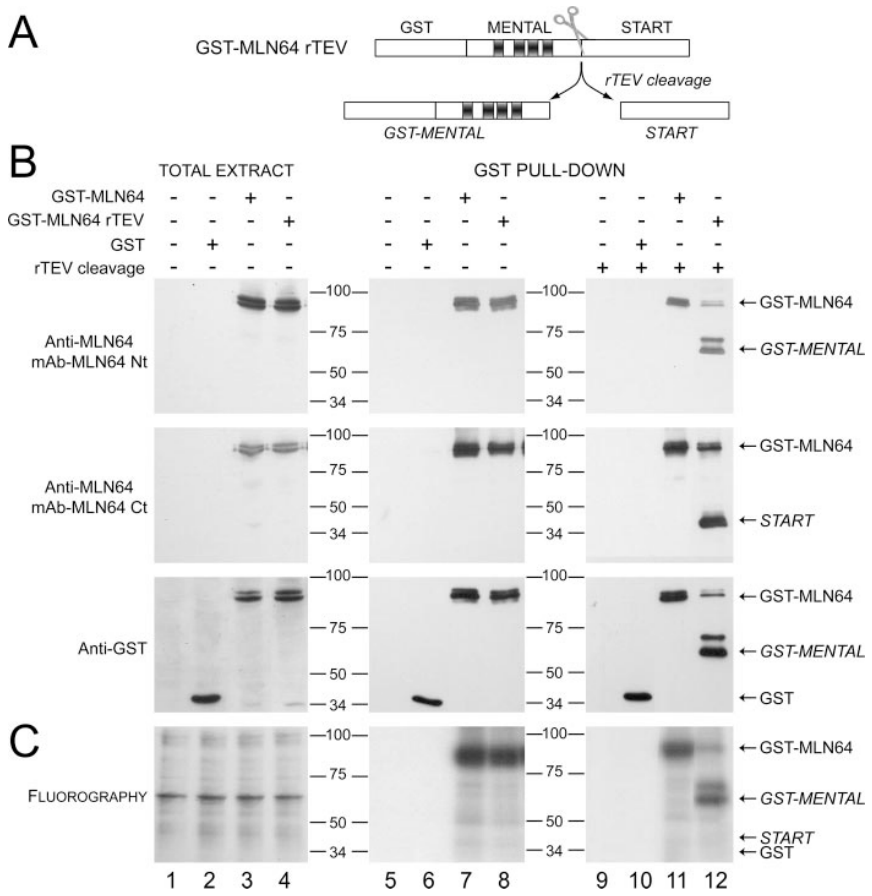


FIG. 5. **The MENTAL domain binds cholesterol.** *A*, scheme of the GST-MLN64-rTEV fusion protein engineered to contain an rTEV cleavage site between the MENTAL and the START domains. After rTEV digestion, the GST-MLN64 protein is cleaved into two fragments corresponding to the GST-MENTAL fusion protein and the START domain. *B*, control HeLa cells (*lanes 1*, *5*, and *9*) or cells transfected with a plasmid encoding GST alone (*lanes 2*, *6*, and *10*), the fusion protein GST-MLN64 (*lanes 3*, *7*, and *11*), or GST-MLN64-rTEV (*lanes 4*, *8*, and *12*) were incubated with [$^3$H]photocholesterol and irradiated with UV light. After cell lysis, total protein extracts were purified by GST pull-down. After washing, half of the bound proteins were cleaved using recombinant TEV. Total protein extracts (*left panel*) and bound proteins before (*middle panel*) or after (*right panel*) rTEV digestion were analyzed by SDS-PAGE, Western blotting, and fluorography. One gel was used to detect proteins by immunoblotting using antibodies directed against the amino-terminal extremity of MLN64 (*mAb-MLN64 Nt*) against the COOH terminus of MLN64 (*mAb-MLN64 Ct*) or against GST protein as indicated on the *left*. *C*, a duplicate gel was used to detect labeled protein-cholesterol complexes using fluorography. The protein molecular size markers are indicated in kDa. The positions of the GST and GST-MLN64 or GST-MLN64-rTEV, GST-MENTAL, and START proteins or fragments are indicated on the *right*.

loops (32). It has recently been shown that the membrane region of sterol regulatory element-binding protein cleavage-activating protein, an important regulator of cholesterol metabolism, is able to bind cholesterol directly (33). Similarly, cholesterol binding to NPC1 was found to need the presence of an intact sterol-sensing domain (34). Using an *in vivo* cholesterol binding assay, we show that the MENTAL domain of MLN64 binds cholesterol. This finding supports the proposed model of MLN64 action on cholesterol transport. MLN64 could capture cholesterol via its MENTAL domain in the late-endosomal membranes, and then cholesterol could be extracted by the cytoplasmic START domain and transferred to a cytosolic acceptor protein or membrane.

The compartmentalization by intracellular organelles and vesicles provide the basis for different cellular functions. Late-endosomal membranes are continuously remodeled in animal cells. Late endosomes are defined by an outer membrane containing discrete protein components (35). Late endosomes also contain internal multivesicular bodies characterized by the distinct composition of their membranes (10). For instance, these internal membranes accumulate specific lipids such as lysobisphosohatidic acid and cholesterol and proteins that are not destined for degradation, such as tetraspanins (36). In mammals, the tetraspanin protein superfamily comprises at least 28 members that are widely expressed (37). These four transmembrane domains-containing proteins aggregate with each other and with a variety of other transmembrane proteins like integrins, major histocompatibility complex class II molecules, signaling complexes, and cell-associated growth factors. Tetraspanins are involved in cell-cell adhesion, migration, assembly of signaling complexes, and modulation of signal transduction (38). Their modes of actions at the molecular level are not clearly understood, but they appear to form large multimeric complexes or microdomains through mutual interactions. It has been suggested that these complexes could be organized in a membrane web involving a network of interacting tetraspanins (39). Although it shares no significant homology with tetraspanin protein sequences, the MENTAL domain also possesses four transmembrane segments. This structural resemblance incited us to examine the possible interaction between MLN64 and MENTHO. Using transiently transfected cells and GST pull-down or co-immunoprecipitation assay, we demonstrate that these interactions are specific because other proteins from late endosomes such as NPC1 or lysosomes such NPC2 fail to interact with the MENTAL domain. Further, FRET studies showed that MENTHO makes homo-dimers or oligomers and interacts with MLN64 in living cells.

Late endosomes form dynamic networks that contain distinct morphologically visible regions and membrane domains (10, 35, 40). MLN64 and MENTHO through homo- and/or hetero-interactions could be involved in the formation of discrete submembrane domains at the surface of late endosomes. In agreement with this finding, MLN64 has been shown to give an uneven staining of the late-endosomal limiting membrane at the ultra-structural level (18). Finally, the overexpression of MENTHO or MLN64 alters the late-endosomal compartment by the formation of less numerous but enlarged endosomes. The exact mechanism is not understood, but we could speculate that overexpression of MLN64 or MENTHO alters the late-endosomal membrane composition through cholesterol sequestration via its MENTAL domain. Our data suggest that, within late-endosomal membranes, MLN64 and MENTHO provide discrete cholesterol-containing domains.

*Acknowledgments*—We thank S. Chan for critical reading of the manuscript, M. Boeglin, D. Hentsch, J. L. Vonesch, and I. Stoll for technical assistance, and S. M. Karam, S. Degot, and D. Massotte for helpful discussion.

REFERENCES

1. Tomasetto, C., Regnier, C., Moog-Lutz, C., Mattei, M. G., Chenard, M. P., Lidereau, R., Basset, P., and Rio, M. C. (1995) *Genomics* **28,** 367–376
2. Bieche, I., Tomasetto, C., Regnier, C. H., Moog-Lutz, C., Rio, M. C., and Lidereau, R. (1996) *Cancer Res.* **56,** 3886–3890
3. Kauraniemi, P., Barlund, M., Monni, O., and Kallioniemi, A. (2001) *Cancer Res.* **61,** 8235–8240
4. Pollack, J. R., Sorlie, T., Perou, C. M., Rees, C. A., Jeffrey, S. S., Lonning, P. E., Tibshirani, R., Botstein, D., Borresen-Dale, A. L., and Brown, P. O. (2002) *Proc. Natl. Acad. Sci. U. S. A.* **99,** 12963–12968
5. Hyman, E., Kauraniemi, P., Hautaniemi, S., Wolf, M., Mousses, S., Rozenblum, E., Ringner, M., Sauter, G., Monni, O., Elkahloun, A., Kallioniemi, O. P., and Kallioniemi, A. (2002) *Cancer Res.* **62,** 6240–6245
6. Dressman, M. A., Baras, A., Malinowski, R., Alvis, L. B., Kwon, I., Walz, T. M., and Polymeropoulos, M. H. (2003) *Cancer Res.* **63,** 2194–2199
7. Moog-Lutz, C., Tomasetto, C., Regnier, C. H., Wendling, C., Lutz, Y., Muller, D., Chenard, M. P., Basset, P., and Rio, M. C. (1997) *Int. J. Cancer* **71,** 183–191
8. Tsujishita, Y., and Hurley, J. H. (2000) *Nat. Struct. Biol.* **7,** 408–414
9. Mukherjee, S., Ghosh, R. N., and Maxfield, F. R. (1997) *Physiol. Rev.* **77,** 759–803
10. Gruenberg, J. (2001) *Nat. Rev. Mol. Cell. Biol.* **2,** 721–730
11. Mellman, I. (1996) *Annu. Rev. Cell Dev. Biol.* **12,** 575–625
12. Brown, M. S., and Goldstein, J. L. (1999) *Proc. Natl. Acad. Sci. U. S. A.* **96,** 11041–11048
13. Soccio, R. E., and Breslow, J. L. (2004) *Arterioscler. Thromb. Vasc. Biol.* **24,** 1150–1160
14. Stocco, D. M. (2001) *Annu. Rev. Physiol.* **63,** 193–213
15. Watari, H., Arakane, F., Moog-Lutz, C., Kallen, C. B., Tomasetto, C., Gerton, G. L., Rio, M. C., Baker, M. E., and Strauss, J. F., III (1997) *Proc. Natl. Acad. Sci. U. S. A.* **94,** 8462–8467
16. King, S. R., Ronen-Fuhrmann, T., Timberg, R., Clark, B. J., Orly, J., and Stocco, D. M. (1995) *Endocrinology* **136,** 5165–5176
17. Arakane, F., Kallen, C. B., Watari, H., Foster, J. A., Sepuri, N. B., Pain, D., Stayrook, S. E., Lewis, M., Gerton, G. L., and Strauss, J. F., III (1998) *J. Biol. Chem.* **273,** 16339–16345
18. Alpy, F., Stoeckel, M. E., Dierich, A., Escola, J. M., Wendling, C., Chenard, M. P., Vanier, M. T., Gruenberg, J., Tomasetto, C., and Rio, M. C. (2001) *J. Biol. Chem.* **276,** 4261–4269
19. Alpy, F., Wendling, C., Rio, M. C., and Tomasetto, C. (2002) *J. Biol. Chem.* **277,** 50780–50787
20. Zhang, M., Liu, P., Dwyer, N. K., Christenson, L. K., Fujimoto, T., Martinez, F., Hanover, J. A., Blanchette-Mackie, E. J., and Strauss, J. F., III (2002) *J. Biol. Chem.* **277,** 33300–33310
21. Millat, G., Marcais, C., Tomasetto, C., Chikh, K., Fensom, A. H., Harzer, K., Wenger, D. A., Ohno, K., and Vanier, M. T. (2001) *Am. J. Hum. Genet.* **68,** 1373–1385
22. Chikh, K., Vey, S., Simonot, C., Vanier, M. T., and Millat, G. (2004) *Mol. Genet. Metab.* **83,** 220–230
23. Thiele, C., Hannah, M. J., Fahrenholz, F., and Huttner, W. B. (2000) *Nat. Cell Biol.* **2,** 42–49
24. Xia, Z., and Liu, Y. (2001) *Biophys. J.* **81,** 2395–2402
25. Parks, T. D., Leuther, K. K., Howard, E. D., Johnston, S. A., and Dougherty, W. G. (1994) *Anal. Biochem.* **216,** 413–417
26. Bose, H. S., Baldwin, M. A., and Miller, W. L. (2000) *Endocr. Res.* **26,** 629–637
27. King, S. R., Ginsberg, S. D., Ishii, T., Smith, R. G., Parker, K. L., and Lamb, D. J. (2004) *Endocrinology* **145,** 4775–4780
28. Tuckey, R. C., Bose, H. S., Czerwionka, I., and Miller, W. L. (2004) *Endocrinology* **145,** 1700–1707
29. Ponting, C. P., and Aravind, L. (1999) *Trends Biochem. Sci.* **24,** 130–132
30. Soccio, R. E., and Breslow, J. L. (2003) *J. Biol. Chem.* **278,** 22183–22186
31. Hanada, K., Kumagai, K., Yasuda, S., Miura, Y., Kawano, M., Fukasawa, M., and Nishijima, M. (2003) *Nature* **426,** 803–809
32. Kuwabara, P. E., and Labouesse, M. (2002) *Trends Genet.* **18,** 193–201
33. Radhakrishnan, A., Sun, L. P., Kwon, H. J., Brown, M. S., and Goldstein, J. L. (2004) *Mol. Cell* **15,** 259–268
34. Ohgami, N., Ko, D. C., Thomas, M., Scott, M. P., Chang, C. C., and Chang, T. Y. (2004) *Proc. Natl. Acad. Sci. U. S. A.* **101,** 12473–12478
35. Miaczynska, M., and Zerial, M. (2002) *Exp. Cell Res.* **272,** 8–14
36. Gruenberg, J. (2003) *Curr. Opin. Cell Biol.* **15,** 382–388
37. Hemler, M. E. (2001) *J. Cell Biol.* **155,** 1103–1107
38. Hemler, M. E. (2003) *Annu. Rev. Cell Dev. Biol.* **19,** 397–422
39. Charrin, S., Manie, S., Billard, M., Ashman, L., Gerlier, D., Boucheix, C., and Rubinstein, E. (2003) *Biochem. Biophys. Res. Commun.* **304,** 107–112
40. Mukherjee, S., and Maxfield, F. R. (2000) *Traffic* **1,** 203–211